Physics Letters B 797 (2019) 134809

Contents lists available at ScienceDirect

Physics Letters B

www.elsevier.com/locate/physletb

The *s*-process in the Nd-Pm-Sm region: Neutron activation of ^{147}Pm

C. Guerrero [a,b,*], M. Tessler [c,d], M. Paul [c], J. Lerendegui-Marco [a], S. Heinitz [e], E.A. Maugeri [e], C. Domingo-Pardo [f], R. Dressler [e], S. Halfon [d], N. Kivel [e], U. Köster [g], T. Palchan-Hazan [c], J.M. Quesada [a], D. Schumann [e], L. Weissman [d]

[a] Universidad de Sevilla, Seville, Spain
[b] Centro Nacional de Aceleradores (Universidad de Sevilla-CSIC-Junta de Andalucía), Seville, Spain
[c] Hebrew University, Jerusalem, Israel
[d] Soreq Nuclear Research Center (SNRC), Yavne, Israel
[e] Paul Scherrer Institut (PSI), Villigen, Switzerland
[f] Instituto de Física Corpuscular (CSIC-Universidad de Valencia), Valencia, Spain
[g] Institut Laue-Langevin (ILL), Grenoble, France

ARTICLE INFO

Article history:
Received 6 February 2019
Received in revised form 25 July 2019
Accepted 25 July 2019
Available online 19 August 2019
Editor: D.F. Geesaman

Keywords:
Nucleosynthesis
Neutron capture
Nuclear reactions
s-process
MACS
Neutron activation

ABSTRACT

The Nd-Pm-Sm branching is of interest for the study of the *s*-process, related to the production of heavy elements in stars. As ^{148}Sm and ^{150}Sm are *s*-only isotopes, the understanding of the branching allows constraining the *s*-process neutron density. In this context the key physics input needed is the cross section of the three unstable nuclides in the region: ^{147}Nd (10.98 d half-life), ^{147}Pm (2.62 yr) and ^{148}Pm (5.37 d). This paper reports on the activation measurement of ^{147}Pm, the longest-lived of the three nuclides. The cross section measurement has been carried out by activation at the SARAF LiLiT facility using a 56(2) μg target. Compared to the single previous measurement of ^{147}Pm, the measurement presented herein benefits from a target 2000 times more massive. The resulting Maxwellian Averaged Cross Section (MACS) to the ground and metastable states in ^{148}Pm are 469(50) mb and 357(27) mb. These values are 41% higher (to the ground state) and 15% lower (to the metastable state) than the values reported so far, leading however to a total cross section of 826(107) mb consistent within uncertainties with the previous result and hence leaving unchanged the previous calculation of the *s*-process neutron density.

1. Introduction and motivation

Most of the elements in our universe are produced in a nucleosynthesis process in the stars that consists of a chain of neutron capture reactions and β-decays. This process, known as the slow-neutron-capture (*s*-) process, takes place in AGB (Asymptotic Giant Branch) stars: low- and intermediate-mass stars late in their life with a structure characterized by an inert core of carbon and oxygen surrounded by burning shells of helium and hydrogen. The description of the *s*-process was formulated in the seminal paper of Burbidge et al. [4], it involves detailed stellar modelling and is constrained by spectroscopic observations. In the context of the stellar modelling, reliable information on the nuclear physics side, half-lives and neutron capture cross sections [12] constitute essential ingredients. In particular, cross sections of several unstable isotopes are of interest because they act as branching points along the *s*-process path where two processes compete: neutron capture and β-decay. This means that if the rates of neutron capture and β-decay in a given branching-point region are known and this information is combined with observed *s*-process isotopic abundances, one can learn about the physical conditions of the stellar site.

For instance, Neyskens et al. [16] have recently been able to determine an upper-limit of 2.5×10^8 K for the *s*-process temperature in low-mass AGB stars (see also Ref. [1]). In their study they used the new experimental values of the unstable ^{93}Zr neutron capture cross section [22] for their model in order to estimate the Zr/Nb abundance ratio in red giants. Based on the dependence of this ratio on the temperature in the stellar site, they used the new observations from the HERMES spectrograph [19] to constrain the *s*-process temperature in low-mass AGB stars.

* Corresponding author at: Facultad de Física, Universidad de Sevilla, Av. Reina Mercedes s/n, 41012 Sevilla, Spain.
E-mail address: cguerrero4@us.es (C. Guerrero).

https://doi.org/10.1016/j.physletb.2019.134809

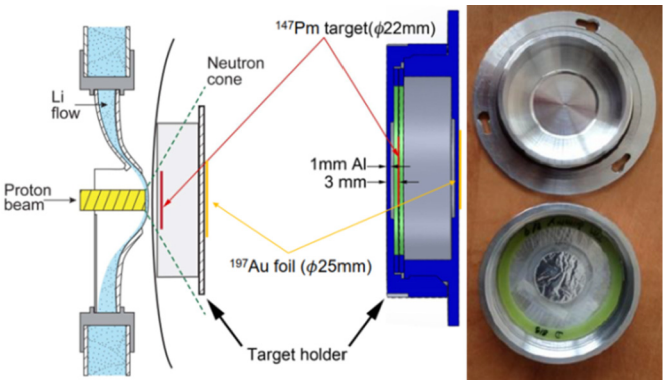

Fig. 1. Left. Schematic diagram of the activation setup: the ^{147}Pm target in an airtight Al holder is located just downstream of the curved wall (thick solid line) separating the vacuum of the LiLiT chamber and that of the activation chamber. Right. Photograph of a dummy target assembly with the holder open: in the actual target the ^{147}Pm deposit is sandwiched between the two thin aluminium layers located at the center of the holder.

In previous work related to the branching in the region $A = 147/148$, Reifarth et al. [21] estimated a value of $4.9(5) \times 10^8$ cm^{-3} for the neutron density in the He-burning shell of low-mass AGB stars from their measured values of the ^{147}Pm$(n,\gamma)^{148g,m}$Pm reactions cross sections, which was the only measurement to date. However, this measurement was made with only 28.7 ng of ^{147}Pm which required using a close geometry detection set-up and measuring decay cascades instead of individual γ-rays. Now that a possibility has arisen to produce a high purity ^{147}Pm target of much higher (2000 times more) mass (see Section 2), a new activation experiment has been carried out in order to provide an independent and more accurate cross section value. The higher target mass combined with the higher neutron flux available allow for a simplified detection set-up, described in Section 2.

2. Cross section measurement

2.1. The promethium target

The high quality of the ^{147}Pm target has been key in the success of the experiment presented herein (see full details about the preparation and characterization of the target in Ref. [9]). In the context of a larger project involving the production of ^{79}Se, ^{163}Ho, ^{171}Tm and ^{204}Tl targets as well, two pellets of $^{146}Nd_2O_3$ enriched to 98.8% and weighing together 98.2 mg were irradiated for 54 days with a thermal flux of 10^{15} n/cm^2/s during the summer of 2013 in the V4 position of the ILL high flux reactor. Neutron capture reactions on ^{146}Nd produced sizable quantities of ^{147}Nd that rapidly decayed into ^{147}Pm. Following chemical separation and purification at PSI, the ^{147}Pm was deposited in circular areas (22 mm in diameter) onto two 5 μm thick Al foils, each glued onto a 6 μm Mylar foil, then placed face-to-face into a 60 mm diameter plastic ring that served as the target holder (Fig. 1). The large diameter of the supporting ring was chosen to make the target usable at the n_TOF facility [7], where the ring must be kept outside the 50 mm diameter neutron beam. The characteristics of the targets employed are summarized in Table 1. The isotopic composition of the ^{147}Pm target was assessed at PSI by ICP-MS and γ-ray spectroscopy after the target preparation. The activity of ^{148m}Pm ($t_{1/2} = 41.3$ d), also produced in the initial activation at ILL, was measured by γ-ray spectroscopy at SARAF prior to the irradiation, using the same setup and methods used later for the SARAF-LiLiT activated target. This was necessary in order to obtain an accurate value to be subtracted (as background) from the ^{148m}Pm activity measured after the SARAF-LiLiT irradiation (Table 1).

Table 1
Characteristics of the targets. The composition of the ^{147}Pm target [9] corresponds to April 18th 2016, the day of the irradiation at LiLiT (~3 years after the irradiation at ILL). The ^{148m}Pm activity quoted here was measured at SARAF prior to the irradiation. Δ denotes the relative uncertainty.

	Ø (mm)	N (atoms)	A (GBq)	Mass (mg)	Δ (%)
Au_{ref}	22	–	–	102.1	0.1
$Au_{mon\text{-}Pm}$	25	–	–	118.8	0.1
$Au_{mon\text{-}Au}$	25	–	–	109.6	0.1
^{147}Pm	22	2.3×10^{17}	1.93	0.056	4.3
^{148m}Pm		3.0×10^{7}	5.6×10^{-9}		3.3
^{146}Nd		3.1×10^{14}	–		12
^{147}Sm		6.6×10^{16}	–		4.3

The irradiations at LiLiT (see next section) take place in vacuum and thus, for safety, the radioactive target was inserted in an airtight target holder illustrated in Fig. 1.

The cross section of ^{147}Pm has been measured in reference to that of ^{197}Au, since both the stellar neutron capture cross section of ^{197}Au [14] and the parameters of the ^{198}Au decay [24] are accurately known. A 118.8(1) mg gold target, 12.5 μm thick 25 mm in diameter ($Au_{mon\text{-}Pm}$) used as a neutron monitor was attached to the back (downstream) of the target holder during the ^{147}Pm irradiation (see Fig. 1). In order to determine the ratio in neutron flux and neutron energy distribution intercepting the ^{147}Pm and Au targets, f_{geom}, another irradiation was made using gold targets of 22 mm (Au_{ref}) and 25 mm ($Au_{mon\text{-}Au}$) in diameter in exactly the same positions as the Pm and $Au_{mon\text{-}Pm}$ ones, respectively. The ratio between the activities induced in these targets together with detailed simulations of the setup (see next section) determined the factor f_{geom}.

2.2. Neutron irradiation at the SNRC Liquid Lithium Target (LiLiT) facility

At the Soreq Nuclear Research Center (SNRC), the SARAF accelerator [13] features a high current (up to 2 mA) low energy (~1.5–4 MeV) proton beam used for neutron production at an energy close to the ^{7}Li(p,n) reaction threshold [20,23]. In order to withstand the high power deposition (3–4 kW), the Liquid-Lithium Target (LiLiT) [8,23,18] is used, consisting of a windowless film (1.5 mm thick, 18 mm wide) of liquid lithium circulating in a closed loop at 2–3 m/s, serving both for neutron production and as the beam dump.

The sketch in Fig. 1 shows the target and activation set-up and includes details on both the liquid lithium target and the target holder at the irradiation position, with the target holder placed at 6 mm from the lithium target surface and the target 3 mm further downstream.

The energy of the proton beam during the irradiation was kept at 1930 keV with a r.m.s. of 15 keV. In this configuration and with the geometry depicted in Fig. 1, the flux and energy distribution of the neutron beam at the target position were estimated via a Monte Carlo simulation using the SimLiT-Geant4 code [6,23]. The result, shown in Fig. 2, resembles a Maxwell-Boltzmann distribution at 40.1 keV with an average neutron flux of 5.47×10^9 cm^{-2} s^{-1} mA^{-1} with a slight reduction of the high energy component, as is common in experiments using the ^{7}Li(p,n) reaction.

The irradiation lasted 4.6 hours during which the neutron beam intensity was monitored with a commercial ^{235}U fission chamber (PFC16A, Centronic Ltd., UK) located just downstream the activation vacuum chamber, and with gamma dosimeters and a $LaBr_3$ scintillation detector attached to the adjacent walls. The corresponding fission count rate, displayed in Fig. 3, shows that follow-

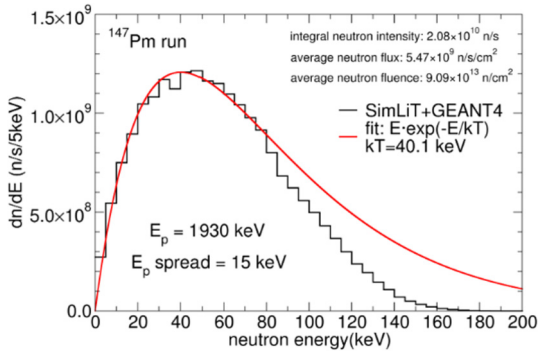

Fig. 2. Simulated neutron spectrum impinging on the ^{147}Pm target according to the SimLiT-Geant4 simulations, including a fit to a Maxwell-Boltzmann distribution at 40.1 keV.

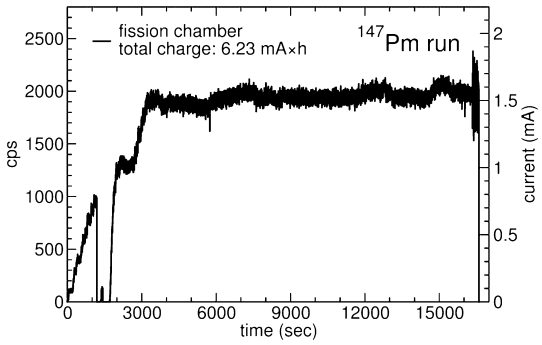

Fig. 3. Counting rate (left axis) of the fission chamber recorded during the irradiation of the ^{147}Pm target. The right axis shows the corresponding charge current.

ing a slow ramp-up of nearly one hour, the beam intensity remained quite constant along the full length of the irradiation. The right axis shows the corresponding proton beam current, based on a calibration performed at low intensity with a Faraday cup in front of the Li target.

2.3. HPGe detection set-up

The gamma spectrometry of the activated Pm and Au (see next section) targets was performed at SARAF with a shielded High-Purity Ge coaxial detector (Ortec GMX25-83, Ser. No. 53-N13229A).

The ^{147}Pm target was kept inside the aluminium holder and placed at 55 mm from the 500 μm thick Be window of the detector. A shielding made of 2 mm of Cu and 6 mm of Pb was installed between the target and the detector in order to minimize the background from low energy photons from the target and from bremsstrahlung related to the β-decay. The irradiated gold targets were placed directly in front of the detector at a distance of 50 mm.

The photopeak efficiency of the detector in the full energy range of interest and in both configurations was determined by measuring the spectrum of certified calibration point sources positioned identically and with an identical holder as the irradiated ^{147}Pm (using ^{152}Eu and ^{60}Co sources) and ^{197}Au (using ^{22}Na, ^{57}Co, ^{60}Co, ^{88}Y, ^{133}Ba, ^{152}Eu, ^{155}Eu and ^{241}Am sources) targets. The distance between the sources and the Ge detector and the heavy shielding of the low-energy ^{152}Eu γ-rays make summing corrections negligible. The efficiency curves are shown in Fig. 4. Given the complexity of absorber setup and target holder, the reliability of the efficiency values has been assessed by comparing the activity of an activated gold target measured in the three configurations mentioned in the legend of Fig. 4, indicating an uncertainty of 5%

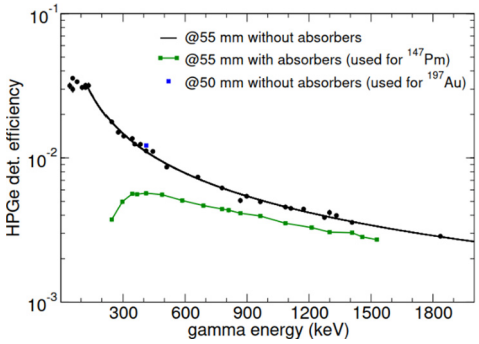

Fig. 4. Efficiency curves of the HPGe detector at 55 mm distance used for the ^{147}Pm target (with and without absorbers) and at 50 mm distance used for ^{197}Au.

and 1.8% in the efficiency for the ^{147}Pm and ^{197}Au targets configurations, respectively. The correction associated to the difference between the detection efficiency for point like (calibration sources) and extended (22/25 mm diameter targets) sources has been calculated by means of Geant4 Monte Carlo simulations. The efficiency differences are 1.8% and 1.3% for the Au and Pm targets, hence the effect becomes negligible (∼0.5%) when the activity of ^{148}Pm is normalized to that of ^{198}Au.

3. Analysis and results

3.1. Gamma activity of the ^{147}Pm and ^{197}Au targets

The number of neutron captures on ^{147}Pm and ^{197}Au during the irradiation is determined from the resulting activities of ^{148}Pm and ^{198}Au, respectively. In the case of capture on ^{147}Pm, the product of the reaction can be formed in the ground (^{148g}Pm) or a metastable (^{148m}Pm) 138 keV state, with quite different half-lives of 5.368(2) d and 41.29(11) d, respectively. While the decay of ^{198}Au [24] is dominated by the emission of a single photon of 412 keV, the decay from ^{148}Pm [17] is more complex with cascades of several γ-rays that in some cases show up in both the decay of the ground and the metastable states of the nucleus (see Fig. 5). The transitions studied, listed in Table 2, are both sufficiently intense and well separated from background lines (see Fig. 6).

The γ-ray spectrum measured with the HPGe detector is shown in Fig. 5, which includes a zoom (right) of two of the γ-rays of interest. The zooms include the spectra recorded before the irradiation at LiLiT, with the spectra after the LiLiT activation downscaled to the counting time of the pre-LiLiT spectra, showing (top right panel) the pre-existing ^{148m}Pm contribution that needs to be subtracted from the irradiated spectra.

Each peak of interest has been fitted to a Gaussian on top of a linear background in order to determine the number of counts (C) in the peak. A series of 24 hour long measurements of the γ-ray lines from ^{148}Pm were carried out over the twelve days following the irradiation. During the first few days after the irradiation, most γ-ray lines were heavily affected by activation background, but as illustrated in Fig. 6, after five days the decay curves correspond to that expected from the decay of ^{148g}Pm and ^{148m}Pm. This confirms the belonging of the different transitions to the decay from the two states as listed in Table 2. The 550 and 915 keV transitions are a special case, as they appear in the decay from both states and hence the decay curve is the sum of two exponential decays, and has been analysed as such. One last point that needs to be considered is the isomeric transition from the metastable to the ground state with a probability of 0.042(6) [17]. This is such that after 12 days of decay, 4% of the activity from the ground state is

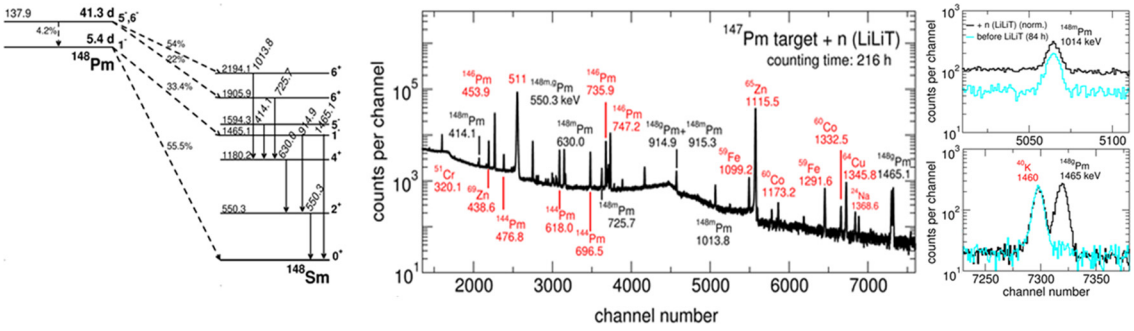

Fig. 5. The transition lines for ^{148g}Pm and ^{148m}Pm studied in this work are indicated in the decay scheme (left), where all the energies are in keV. The corresponding γ-ray spectrum of the ^{147}Pm target after activation, recorded at a distance of 55 mm from the HPGe detector with the absorber configuration described in the text, shows the mentioned transition lines and others from activated contaminants (marked in red); the activity from ^{144}Pm and ^{146}Pm in the same amount as before the irradiation. The zoom spectra in the right panel correspond to the regions of the 1013.8 and 1465.12 keV photopeaks from the decay of ^{148m}Pm and ^{148g}Pm, respectively. In these spectra, the measurement after LiLiT activation is downscaled to the counting time of the pre-LiLiT spectra, where the ^{148m}Pm contribution prior to the irradiation can be observed.

Table 2
γ-Ray lines energies, intensities, associated detector efficiencies and γ-ray attenuation in the corresponding target for the transitions studied in the decay of ^{198}Au, ^{148g}Pm and ^{148m}Pm [24,17]. The intensities given are absolute, hence are those listed in the references normalized to those of the reference γ-ray lines of 411.80, 1465.12, 629.97 keV lines in the decay of ^{198}Au, ^{148g}Pm and ^{148m}Pm, respectively. The R_{EOI} values are the result of the fits displayed in Fig. 6. All the reported uncertainties are systematic, the statistical ones of the measurement displayed in Fig. 6 range between 1% and 3%, becoming negligible when all the data points are considered in the fit.

	^{198}Au$_{\text{mon-Pm}}$	^{148g}Pm			^{148m}Pm						
E_γ (keV)	411.8020(2)	550.27(3)	914.85(6)	1465.12(3)	414.07(6)	550.27(3)	599.74(6)	629.97(3)	725.70(3)	915.33(6)	1013.81(3)
Intensity I_γ (%)	95.62(6)	22.0(5)	11.5(5)	22.2(5)	18.7(2)	94.9(12)	12.5(2)	89.0(9)	32.8(4)	17.2(2)	20.3(3)
Efficiency ε (%)	1.22(2)	0.517(15)	0.392(11)	0.281(8)	0.549(16)	0.517(15)	0.498(14)	0.486(15)	0.449(13)	0.392(11)	0.367(11)
γ-ray att. C_{att} (%)	0.3	2.2	1.5	1.4	2.4	2.2	2.2	2.1	2.0	1.5	1.6
R_{EOI} (s^{-1})	317(1)	0.038(3)	0.013(2)	0.0210(2)	0.00854(12)	0.046(1)	0.00538(10)	0.0378(3)	0.0142(2)	0.0065(10)	0.0062(1)
N^*_{EOI} (10^7)	947(18)	2.30(18)	1.9(3)	2.26(18)	4.42(6)	4.96(11)	4.59(8)	4.60(4)	5.07(7)	4.8(7)	4.36(7)
N^*_{EOI} (10^7) (avg.)	947(18)	2.2(2)			4.7(2)						

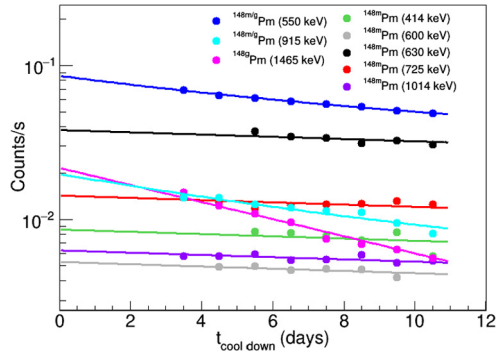

Fig. 6. Decay curves of ^{148}Pm from its ground (g) and metastable (m) states. The measured data (markers) correspond to average daily values and the lines to the corresponding fits (see text for details).

due to this contribution. The associated correction to the measured activity from the ground state is 1.7(3)%.

The fits provide the estimated value of the counting rate (R_{EOI}) for each peak at the end of the irradiation (EOI), from which the number of nuclei N_{EOI} can be calculated as:

$$N_{EOI} = \frac{R_{EOI}}{\lambda \varepsilon I_\gamma (1 - C_{att})},$$

taking into account for each line the decay constant (λ), correction associated to the attenuation of the γ-rays (C_{att}), efficiency (ε) and γ-ray intensities (I_γ) mentioned above. The results for Pm and the reference Au target are summarized in Table 2, where it is shown that the results in terms of N_{EOI} calculated from the different transition lines of ^{148}Pm are compatible. The level of agreement is ∼4% for the seven transitions from ^{148m}Pm and within 9% for the three lines from ^{148g}Pm.

3.2. Determination of the Maxwellian Averaged Cross Section (MACS) of ^{147}Pm

The cross section of ^{147}Pm is determined taking as reference the JEFF-3.3 [11] evaluation of ^{197}Au. This evaluation features a cross section compatible with the recent standard MACS value of 612 mb at 30 keV [5], which is 6% larger than the previous value of Ratynski and Käppeler [20], used as reference in all activation measurements between 1988 and 2011. In particular, what is used as reference is the spectrum averaged cross section (SACS) of ^{197}Au, i.e. the convolution of the evaluated point-wise cross section [11] with the neutron energy distribution at LiLiT, determined from the SimLiT-GEANT4 simulations:

$$\langle \sigma(^{197}\text{Au}) \rangle_{LiLiT} = \frac{\int \sigma_{JEFF3.3}(\text{Au}, E_n) \frac{dn_{sim}}{dE_n} dE_n}{\int \frac{dn_{sim}}{dE_n} dE_n} = 533(9)\ \text{mb}$$

SimLiT [6] uses experimentally determined ^{7}Li(p,n) cross sections, two-body kinematics and proton energy loss in the Lithium target as well as the energy spread of the proton beam, to calculate neutron spectra, intensities and angular distributions. Combined with Geant4 [2] for the neutron transport, it allows simulating the neutron intensity and energy distribution intersecting the target of interest [23], in this case the Au and Pm targets, each at a different position and with a different diameter. The simulation allows as well determining the geometric effect (f_{geom}) of the different flux (lower intensity and slightly higher neutron energy) intersecting the Au and Pm targets. The experimental value for f_{geom} of 0.232(7), resulting from the analysis of the Au$_{\text{ref}}$ and Au$_{\text{mon-Au}}$ targets, agrees within 3% with that obtained from the simulations.

Using as reference the experimental cross section of ^{197}Au, the experimental capture cross section going to each of the ^{148}Pm states is calculated as:

Table 3
MACS values at different neutron energies, i.e. stellar temperatures. The uncertainty estimated at 30 keV has not been extrapolated to other thermal energies.

E_n (keV)	5	10	15	20	25	30	40	60	80	100
MACS (b)	2.6	1.7	1.2	0.98	0.92	0.826(107)	0.69	0.58	0.51	0.50

$$\langle\sigma\left(^{147\rightarrow 148x}\mathrm{Pm}\right)\rangle_{LiLiT} = \langle\sigma\left(^{197}\mathrm{Au}\right)\rangle_{LiLiT}\frac{N_{EOI}(^{148x}\mathrm{Pm}) - N_0(^{148x}\mathrm{Pm})}{N_{EOI}(^{198}\mathrm{Au_{mon\text{-}Pm}})} \times \frac{N_0(^{197}\mathrm{Au_{mon\text{-}Pm}})}{N_0(^{147}\mathrm{Pm})} f_{geom},$$

which gives:

$$\langle\sigma\left(^{147\rightarrow 148g}\mathrm{Pm}\right)\rangle_{LiLiT} = 460(49)\ \mathrm{mb},$$
$$\langle\sigma\left(^{147\rightarrow 148m}\mathrm{Pm}\right)\rangle_{LiLiT} = 350(38)\ \mathrm{mb},$$

However, the quantity of interest in the nucleosynthesis network calculations within the stellar evolution models is the Maxwellian Average Cross Section, or MACS, at a given temperature. In the stellar interior, the neutrons are considered to be in thermal equilibrium with the medium at a characteristic value of kT. Hence, the neutron capture reaction rate is given by $\langle\sigma\upsilon\rangle$, the convolution of the product of the cross section times the relative velocity over the distribution of neutrons at the given kT. Considering the most probable velocity υ_T, the MACS is then defined as:

$$\langle\sigma\rangle_{kT} = \frac{\langle\sigma\upsilon\rangle}{\upsilon_T} = \frac{2}{\sqrt{\pi}}\langle\sigma\rangle = \frac{2}{\sqrt{\pi}}\frac{\int\sigma(E_n)E_n e^{-E_n/kT}dE_n}{\int E_n e^{-E_n/kT}dE_n}$$

Since the energy distribution of the neutron flux incident on the targets at LiLiT is fitted reasonably well by a Maxwellian distribution, the experimental cross section can be extrapolated into the MACS as (see [23] for details):

$$\langle\sigma\left(^{147}\mathrm{Pm}\right)\rangle_{kT} = \frac{2}{\sqrt{\pi}}C_{E_n}(kT)\langle\sigma\left(^{147}\mathrm{Pm}\right)\rangle_{LiLiT},$$

with the correction factor:

$$C_{E_n}(kT) = \frac{\int_0^\infty\sigma(^{147}\mathrm{Pm}, E_n)E_n e^{-\frac{E_n}{kT}}dE_n}{\int_0^\infty E_n e^{-\frac{E_n}{kT}}dE_n} \times \frac{\int_0^\infty\frac{dn_{sim}}{dE_n}dE_n}{\int_0^\infty\sigma(^{147}\mathrm{Pm}, E_n)\frac{dn_{sim}}{dE_n}dE_n}$$

accounting for the difference between the convolution of the evaluated ^{147}Pm cross section (similar in JEFF-3.3 and ENDF/B-VIII.0 [10]) with the neutron distribution at LiLiT and with a Maxwell-Boltzmann distribution at the chosen temperature. The value of C_{En} at 30 keV is 1.02(2), a value very close to unity owing to the resemblance of the neutron energy distribution at LiLiT with that of the Maxwellian of interest. The uncertainty of C_{En} is estimated from the deviations of the results for different libraries and is quite small because C_{En} depends only on the shape, and not the absolute value of the cross section.

The resulting partial MACS values at 30 keV are:

$$\langle\sigma\left(^{147\rightarrow 148g}\mathrm{Pm}\right)\rangle_{30\ \mathrm{keV}} = 469(50)\ \mathrm{mb},$$
$$\langle\sigma\left(^{147\rightarrow 148m}\mathrm{Pm}\right)\rangle_{30\ \mathrm{keV}} = 357(27)\ \mathrm{mb},$$

resulting in the total MACS of:

$$\langle\sigma\left(^{147}\mathrm{Pm}\right)\rangle_{30\ \mathrm{keV}} = 826(107)\ \mathrm{mb}.$$

Table 4
Summary of the experimental values for the partial and total MACS values for the ^{147}Pm(n,γ) reaction.

	$\langle\sigma(^{147\rightarrow 148g}\mathrm{Pm})\rangle_{30\ \mathrm{keV}}$	$\langle\sigma(^{147\rightarrow 148m}\mathrm{Pm})\rangle_{30\ \mathrm{keV}}$	Ratio (g/m)
This work	469(50) mb	357(27) mb	1.31
Reifarth et al.[+]	332(64) mb	419(58) mb	0.79
Difference	+41%	−15%	

[+] Original values scaled up by 6% because of the new ^{197}Au standard [5].

Regarding the partial contributions to the overall systematic uncertainty, the dominant components are the 4.3% of the ^{147}Pm target mass (see Table 1), the 2%, 4% and 9% in the calculated number of ^{198}Au, ^{148m}Pm and ^{148g}Pm nuclei (see Table 2), the 3% in the correction related to the different beam intensity intersecting the Pm and the monitor Au target (f_{geom}) and, in the case of capture to ^{148m}Pm, the 3% related to the amount of ^{148m}Pm in the target before the irradiation at LiLiT.

The neutron energy of 30 keV is generally chosen for measuring and reporting MACS values, but the cross section to be used in the nucleosynthesis calculations depends on the temperature of the stellar site. Hence, we report in Table 3 as well the MACS value at other neutron energies, calculated from the corresponding value of C_{En}.

4. Discussion

The quantities measured in this work are the neutron capture cross sections to the ground and metastable states in ^{148}Pm. The values reported herein are, as summarized in Table 4, significantly different from the only other values available in the literature [21]: 41% larger and 15% smaller than the MACS to the ground and metastable states, respectively. The experiment of Reifarth used a 4π geometry with two Clover-type HPGe detectors for measuring in coincidence pairs of γ-rays corresponding to the decay from ^{148g}Pm or ^{148m}Pm. In the case of the decay from the ground state the results are based only in a single cascade (550/915 keV), hence without the possibility to be cross checked, while our work combines the results from three independent γ-ray transitions that agree within 9%. Indeed, our values (see Table 2) show a sizable (∼20%) deviation of the results for the 915 keV compared to the 550 and 1465 keV lines, which may hint to an inaccuracy in the corresponding transition intensity to which the measurements of Reifarth would be much more sensitive. Regarding the capture to ^{148m}Pm, our cross section results from the combination of seven γ-ray transitions whose results agree within 4%, while the value of Reifarth et al. is the combination of measuring three cascades but no information is given about the level of agreement between them.

In nucleosynthesis calculations, the strength of a branching can be calculated from the rate for β-decay and neutron capture of the branch point nucleus:

$$f_b = \frac{\lambda_\beta}{\lambda_\beta + \lambda_n}$$

In the case of interest, ^{148}Pm, the β-decay rate is quite different (a factor of 8) for the ground and metastable state. Hence, the very different ratio of capture to the ground and metastable states found in this work (1.31) with respect to the previous experiment

(0.79) could have a large effect on the corresponding neutron density calculation. However, Lesko et al. [15] showed that at the temperature of the *s*-process the ground and the metastable state are thermally equilibrated and the effective half-life at 3.5×10^8 K (i.e. 30 keV) is 5.6 days, slightly larger than that of the metastable state. Therefore, what matters in nucleosynthesis calculations is the total and not the partial cross sections. In this work we report a total cross section at 30 keV of 826(107) mb, 35% lower than the theoretical and evaluated cross sections, which combined give a value of 1290(470) mb [3]. On the other hand, our total cross section value is 11% higher, but in agreement within uncertainties, with the value of 744(100) of Reifarth et al. Therefore the neutron density of $4.9(5)10^8$ calculated from the network around the $A = 147/148$ branching in Ref. [21] remains valid according to our results.

A further step in the understanding of the branching in the $A = 147/148$ region would require the measurement of the other two unstable isotopes involved: ^{147}Nd and ^{148}Pm. However, their short half-lives of just 10.98 and 5.37 days, respectively, and the difficulties associated to producing a suitable target in terms of mass do not allow measuring their capture cross section with the current techniques.

5. Conclusions

Neutron capture on some radioactive isotopes along the *s*-process path is key for determining the stellar conditions where the majority of the elements of the universe are produced. However, the related cross sections are very difficult to measure, as this requires both enough target mass and a very intense neutron beam of the proper energy distribution. In this work, the highest mass ^{147}Pm target to date has been produced at the ILL high flux reactor and fabricated at PSI, resulting in a 56(2) μg target, about 2000 times larger than that of the 28.7(12) ng target used in the only previous experiment. In spite of this, the ^{147}Pm target is the smallest-mass and shortest-lived isotope measured to date at LiLiT.

The target was irradiated with the quasi-stellar neutron beam of the LiLiT facility at SARAF at the Soreq NRC in Israel, and the induced activity was measured with a HPGe detector. The results from the analysis of several γ-ray transitions from both the ground (5.4 days) and the metastable (41.3 days) states of the unstable ^{148}Pm yield a MACS value at 30 keV of 826(107) mb, with contributions of 469(50) and 357(27) mb from the ground and metastable states, respectively. These partial cross sections are significantly different (−15% and +41%) from the only other experimental values available. However, for the particular case of ^{147}Pm(n,γ) what matters is the total capture cross section and in this work we have confirmed within uncertainties the value of Reifarth et al., therefore confirming as well the neutron density calculations given in Ref. [21].

Acknowledgements

The authors acknowledge financial support by University of Seville via the VI PPIT-US programme, the Spanish FPA2013-45083-P, FPA2014-53290-C2-2-P and FPA2016-77689-C2-1-R projects, and the EC FP7 projects NeutAndalus (Grant No. 334315) and CHANDA (Grant No. 605203) and the CERN n_TOF Collaboration. The SARAF-LiLiT experiment was supported by the PAZY Foundation (Israel). M.P. acknowledges support of the Israel Science Foundation (Grant No. 1387/15).

References

[1] C. Abia, et al., Astrophys. J. 559 (2016) 1117–1134.
[2] S. Agostinelly, et al., Nucl. Instrum. Methods A 506 (2003) 250–303.
[3] Z.Y. Bao, et al., At. Data Nucl. Data Tables 76 (2000).
[4] E.M. Burbidge, G.R. Burbidge, W.A. Fowler, F. Hoyle, Rev. Mod. Phys. 29 (1957) 547.
[5] A.D. Carlson, et al., Nucl. Data Sheets 148 (2018) 143–188.
[6] M. Friedman, et al., Nucl. Instrum. Methods A 698 (2013) 117.
[7] C. Guerrero, et al., Eur. Phys. J. A 49 (2013) 27.
[8] S. Halfon, et al., Rev. Sci. Instrum. 85 (2014) 056105.
[9] S. Heinitz, et al., Radiochim. Acta 105 (10) (2017) 801–811.
[10] ENDF - IAEA NDS - International Atomic Energy Agency, https://www-nds.iaea.org/endf/.
[11] JEFF-3.3: the joint evaluated fission and fusion file, 2017.
[12] F. Käppeler, R. Gallino, S. Bisterzo, W. Aoki, Rev. Mod. Phys. 83 (2011) 157.
[13] A. Kreisel, et al., LINAC2014 – Proceedings, Geneva, Switzerland, 2014.
[14] C. Lederer, et al., The n_TOF Collaboration, Phys. Rev. C 83 (2011) 034608.
[15] K.T. Lesko, E.B. Norman, R.M. Larimer, J.C. Bacelarand, E.M. Beck, Phys. Rev. C 39 (1989) 619.
[16] P. Neyskens, et al., Nature 517 (2015).
[17] N. Nica, Nucl. Data Sheets 117 (2014) 1–229.
[18] M. Paul, et al., Eur. Phys. J. A 55 (2019) 44.
[19] Raskin, et al., Astron. Astrophys. 526 (2011) A69.
[20] W. Ratynski, F. Käppeler, Phys. Rev. C 37 (1988) 595.
[21] R. Reifarth, et al., Astrophys. J. 582 (2003) 1251.
[22] G. Tagliente, et al., The n_TOF Collaboration, Phys. Rev. C 87 (2013) 014622.
[23] M. Tessler, et al., Phys. Lett. B 751 (2015) 418.
[24] H. Xiaolong, K. Mengxio, Nucl. Data Sheets 133 (2016) 221.